Study on the Luminescence and Energy Level of Lanthanide Ions in Lu0.8Sc0.2BO3 Host

ARTICLE *in* THE JOURNAL OF PHYSICAL CHEMISTRY A · DECEMBER 2011

Impact Factor: 2.69 · DOI: 10.1021/jp209017w · Source: PubMed

THE JOURNAL OF PHYSICAL CHEMISTRY A

ARTICLE

pubs.acs.org/JPCA

Study on the Luminescence and Energy Level of Lanthanide Ions in $Lu_{0.8}Sc_{0.2}BO_3$ Host

Yuntao Wu,*[,†] Guohao Ren,*[,†] Martin Nikl,[‡] Dongzhou Ding,[†] Jiayu Wang,[§] Shanshan Shang,[#] Fan Yang,[†] and Shangke Pan[†]

[†]Shanghai Institute of Ceramics, Chinese Academy of Sciences, No.215 Chengbei Road, Jiading, Shanghai 201800, P. R. China

[‡]Institute of Physics, Academy of Sciences of the Czech Republic, Cukrovarnická 10, 16253 Prague 6, Czech Republic

[§]College of Chemistry, Chemical Engineering and Materials Science, Soochow University, Renai Road No. 199, Suzhou 215123, P. R. China

[#]College of Materials Science, China Jiliang University, Zhejiang 310018, P. R. China

ABSTRACT: Emission and excitation spectra of undoped and Ln^{3+} (Ln = Ce, Pr, Nd, Yb)-doped $Lu_{0.8}Sc_{0.2}BO_3$ were studied by vacuum ultraviolet spectroscopy, and the X-ray excited luminescence spectra were measured as well at room temperature. The undoped specimen presented two different emissions upon excitation at energies in the vicinity of the band gap or with X-ray. The emission at the highest energy side, located at 4.77 eV, was ascribed to self-trapped exciton, which is anchored by electron capture around the Sc site. We also observed three broad emission bands at 4.43, 3.02, and 2.10 eV, which might be attributed to the trapped exciton, defect-related emissions, or both. Energy transfer processes to the doped lanthanide ions in $Lu_{0.8}Sc_{0.2}BO_3$ via exciton state or sequential electron−hole capture are discussed. Finally, the energy level diagram for divalent and trivalent lanthanides in $Lu_{0.8}Sc_{0.2}BO_3$ was constructed using the obtained spectroscopic parameters and the three parameters method (Dorenbos, P. *J. Phys.: Condens. Matter* **2003**, *15*, 8417).

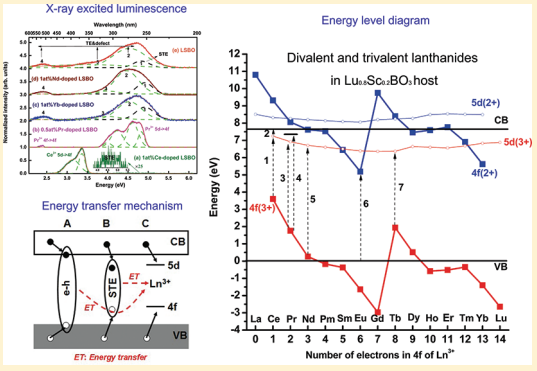

1. INTRODUCTION

Cerium-activated lutetium orthoborate has been identified as a promising scintillator[1−3] due to its high density (~7 g/cm^3), high light yield (over 20 000 ph/MeV), and fast decay time (~30 ns). Although $LuBO_3$:Ln^{3+} (Ln = Ce, Eu, Tb) materials have been recently prepared in the form of scintillation films and composites,[4−8] the high-temperature phase transformation[9−11] makes it hard to obtain bulk $LuBO_3$ single crystal directly from the melt. Recently, it has been found that a Sc^{3+} admixture can stabilize the calcite phase of $LuBO_3$, and the $Lu_{0.9}Sc_{0.1}BO_3$:Ce^{3+} crystals have been proposed for applications in γ-ray detection.[12,13] In our earlier work, the influence of the Sc/Lu ratio on phase transformation and luminescence properties of $Lu_{1-x}Sc_xBO_3$:Ce solid solutions were investigated.[14] Resulting Czochalski-grown Ce-doped lutetium scandium orthoborate single crystals appeared promising scintillators.[15−17]

However, optimization of any scintillator requires good understanding of its scintillation mechanism, including specific defects' occurrence and their role in it. The relationship describing the overall scintillation efficiency, η, could be expressed as $\eta = \beta SQ$,[18,19] where β is the conversion efficiency of an incident photon to form electron−hole pairs, S is the transfer efficiency of the electron−hole pairs to the luminescent center, and Q is the efficiency of luminescence from the center. Among these parameters, S is regarded as the most important and least predictable one (in terms of scintillation efficiency and response).[20] At present, although there are several studies about the optical and scintillation properties of Ln^{3+} in the $Lu_{0.8}Sc_{0.2}BO_3$ host,[16,21,22] three important questions related to the transfer stage of scintillator mechanism (parameter S) have not yet been answered:

(i) What is the origin of the host emission in $Lu_{0.8}Sc_{0.2}BO_3$? Because host emission centers always compete with the doped ones, the scintillation efficiency and response in time are critically dependent on this competition,

(ii) What is the energy transfer mechanism from host to activator in $Lu_{0.8}Sc_{0.2}BO_3$:Ln^{3+}? The existence of an efficient channel of energy transfer from the excited host to the activator is essential for the final scintillation efficiency.

(iii) What is the energy level location of divalent and trivalent ions in the $Lu_{0.8}Sc_{0.2}BO_3$ host? Since the scintillation process strongly depends on the location of the excited state or the ground state of the luminescent center relative to the bottom of the conduction band or the top of the valence band, such knowledge is very important.

Received: September 18, 2011
Revised: October 20, 2011
Published: October 25, 2011

In this paper, we attempt to answer these questions. Both synchrotron radiation excitation used for VUV-UV spectroscopy and X-ray excited radioluminescence are employed to study the properties of pure and several lanthanide ion-doped $Lu_{0.8}Sc_{0.2}BO_3$ specimens. A similar method has been applied for understanding the mechanism of the host-to-activator energy transfer in Lu_2O_3:Eu ceramics.[23] Using a predictive tool proposed by Dorenbos[24] and the spectroscopic experiment results, the energy level diagrams of divalent and trivalent ions in $Lu_{0.8}Sc_{0.2}BO_3$ host are established. This method has been successfully applied for many hosts, such as GaN,[25] $LiYP_4O_{12}$,[26] YPO_4,[27,28] $Lu_2Si_2O_7$.[29] The spectroscopic parameters are derived from the charge transfer transitions in the $Lu_{0.8}Sc_{0.2}BO_3$ doped with Eu^{3+} and Yb^{3+}, and the d−f transitions in $Lu_{0.8}Sc_{0.2}BO_3$ doped with Ce^{3+}, Pr^{3+}, Nd^{3+}, and Tb^{3+}. Furthermore, the photoluminescence and decay time measurements as a function of temperature[30−32] have been utilized to construct the relative energy position between the trivalent lanthanide (Ce^{3+}, Pr^{3+}) lowest 5d state and the conduction band.

2. MATERIALS AND EXPERIMENTS

The calcite phase of $LuBO_3$, $ScBO_3$, $Lu_{0.8}Sc_{0.2}BO_3$ polycrystalline powder specimens were prepared using conventional solid-state reaction method. The reactants include 4N purity Lu_2O_3, Sc_2O_3, and H_3BO_3. Stoichiometric amounts of starting materials were weighed, except for H_3BO_3, which was 5 wt % rich due to vaporization loss in high-temperature synthesis, and then thoroughly mixed and ground. Subsequently, the mixture was calcined at 1200 °C in air for 20 h and gradually cooled down to room temperature.

Ln^{3+}-doped $Lu_{0.8}Sc_{0.2}BO_3$ (Ln = Ce, Pr, Yb, and Nd) single crystals, initially doped with 1 atom % Ce^{3+}, 0.5 atom % Pr^{3+}, 1 atom % Yb^{3+}, or 1 atom % Nd^{3+} were grown by the Czochralski method. Lu_2O_3, Sc_2O_3, CeO_2 (Pr_6O_{11}, Yb_2O_3, Nd_2O_3), and H_3BO_3 with 4N purity were used as raw materials, and stoichiometric amounts of starting materials were weighed, except for H_3BO_3, which was 5 wt % richer than the stoichiometric ratio due to vaporization loss during crystal growth. Mixtures of the raw materials were calcined at 1200 °C for 20 h to initially complete the solid state reaction and then charged in an iridium crucible of dimensions of Ø60 × 40 mm^3. Crystals were grown in Argon atmosphere and with 2 mm/h pulling rate and 10 rpm rotating rate. The dimensions of the ingots obtained were of about 20 mm in diameter and 30 mm in length. After cutting and polishing, small samples of approximate dimensions 2 × 2 × 2 mm^3, which were clear and without visible imperfections, were used for the measurements. The structure of prepared crystals was examined by X-ray powder diffraction using Cu Kα radiation. The XRD data indicated that all the specimens were single calcite phase and in good agreement with PDF cards 79-0097 [$LuBO_3$] and 72-1053 [$ScBO_3$].

The radioluminescence spectra were excited by an X-ray tube at a luminescence spectrometer, assembled at Shanghai Institute of Ceramics. The VUV-UV excitation and emission spectra were measured at the China National Synchrotron Radiation Laboratory (NSRL) VUV spectroscopy workstation on a U24 beamline. The electron energy in the storage ring was kept at 800 MeV, and the beam current was in the range of 100−250 mA. This workstation was equipped with a Seya-Namioka excitation monochromator (1200 g/mm, 100−400 nm), an ACS-257 emission monochromator (1200 g/mm, 200−700 nm), and a Hamamatsu H8259-01 photomultiplier detector. The resolution is ∼0.2 nm. The vacuum in the sample chamber during measurement was kept at ∼1 × 10^{-3} Pa. Excitation spectra were corrected for the spectral shape of the excitation source by means of sodium salicylate reference measurement. All spectra were measured at room temperature.

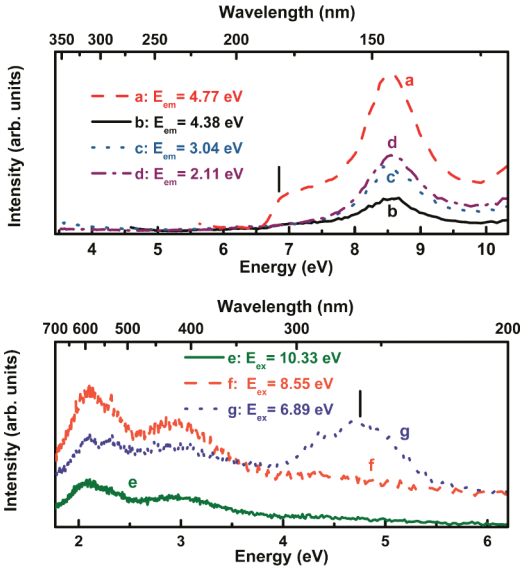

Figure 1. The VUV excitation spectrum (under emission at 4.77 (a), 4.38 (b), 3.04 (c), and 2.11 eV (d)), VUV excited emission spectrum (excitation under 10.33 (e), 8.55 (f), and 6.89 eV (g)) of pure $Lu_{0.8}Sc_{0.2}BO_3$.

3. RESULTS AND DISCUSSION

3.1. Host Emission of Undoped $Lu_{0.8}Sc_{0.2}BO_3$. The VUV excitation and emission spectra of undoped $Lu_{0.8}Sc_{0.2}BO_3$ are shown in Figure 1. In this paper, the band gap is defined as the mobility edge, which is determined by the onset of the valence-to-conduction band transition. In the excitation spectrum, the dominant band with a maximum at 8.55 eV (a−d) can be assigned to the host excitation, and the band gap of $Lu_{0.8}Sc_{0.2}BO_3$ is about 7.6 eV (163 nm). The band gap in other rare earth orthoborates is calculated to be ∼7.0−7.8 eV,[33−35] which is close to our result.

Spectrum "a" has an additional shoulder peaking at about 6.89 eV. Upon excitation at 6.89 eV, the emission spectra consist of four broad bands, peaking at about 4.77, 4.43, 3.02, and 2.10 eV. The first band has been attributed to the self-trapped exciton emission (STE).[16] The other bands could be ascribed to the trapped exciton (TE) or defect-related emissions and are quite visible upon excitation at 10.33 and 8.55 eV. The STE emission peak hardly appears upon excitation at 10.33 and 8.55 eV, characteristic for the band-to-band absorption, which means that migrating free charge carriers are preferably localized around defects, instead, to form a STE.

Let us consider the origin of the STE. In the literature,[36,37] the STE emission at ∼4.59 eV (270 nm) in $Lu_3Al_5O_{12}$:Sc is ascribed to the excitons localized around the Sc site. Zorenko[38] proposed that the TE in $YAlO_3$:Sc emitting at about 290 nm is formed from the 2p-type hole localized at the singly charged O^- ions and electron localized at the mixed 3p-states of Al^{3+} and 3d-states of

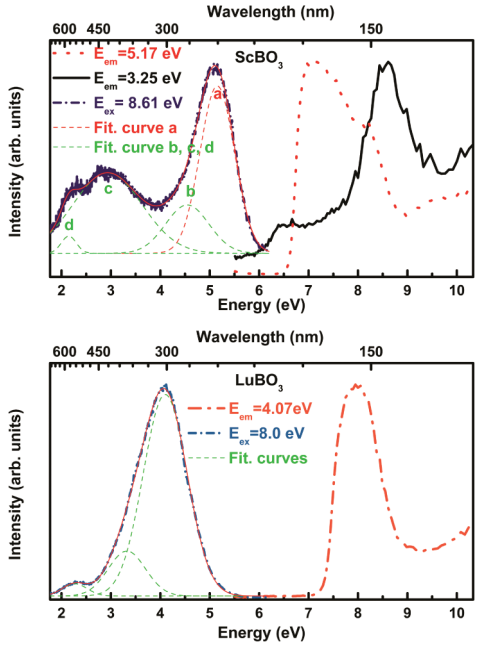

Figure 2. The VUV excitation spectrum and excited emission spectrum of pure calcite phase of $LuBO_3$ and pure $ScBO_3$.

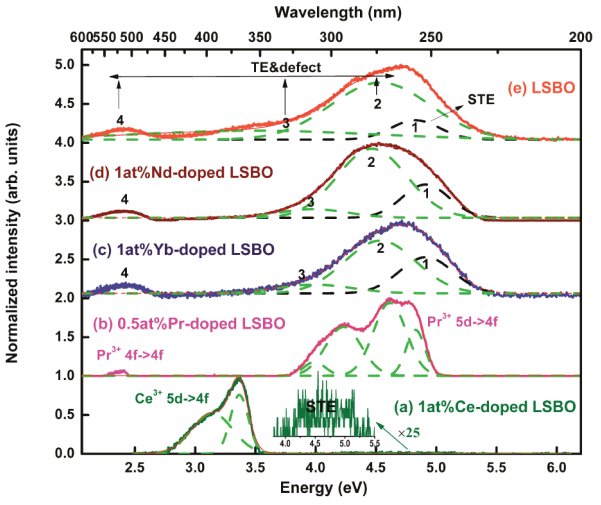

Figure 3. X-ray-excited luminescence spectra at room temperature of $Lu_{0.8}Sc_{0.2}BO_3$:1 atom % Ce (a), $Lu_{0.8}Sc_{0.2}BO_3$:0.5 atom % Pr (b), $Lu_{0.8}Sc_{0.2}BO_3$:1 atom % Yb (c), $Lu_{0.8}Sc_{0.2}BO_3$:1 atom % Nd (d), and pure $Lu_{0.8}Sc_{0.2}BO_3$ (e).

Sc^{3+}. It has been shown that the Sc^{3+} doping in $Lu_3Al_5O_{12}$ gives rise to a deep electron trap.[39] Therefore, we tentatively propose that the STE in $Lu_{0.8}Sc_{0.2}BO_3$ host is formed from the 2p-type hole localized at the singly charged O^- ions and electron localized at the 3d states of Sc^{3+}, where the latter could be an anchoring element in the STE creation.

To further confirm the origin of these host emissions, the VUV excitation and emission of the undoped calcite phase of $LuBO_3$ and $ScBO_3$ were also investigated and are presented in Figure 2. In $ScBO_3$, the emission spectrum under excitation at 8.61 eV could be decomposed into four bands: a, b, c, and d. Monitoring the emission at 5.17 eV (band a), the corresponding excitation

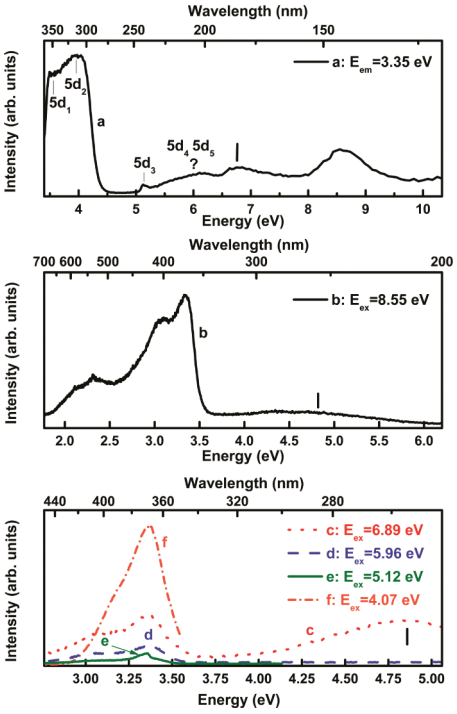

Figure 4. The VUV excitation spectrum (under emission at 3.35 eV (a)) and VUV excited emission spectrum (excitation under 8.55 (b), 6.89 (c), 5.96 (d), 5.12 (e), and 4.07 eV (f)) of $Lu_{0.8}Sc_{0.2}BO_3$:1 atom % Ce.

band with a maximum at 7.1 eV, which is low-energy-shifted compared with excitation bands of the other three emissions (band b, c, d), is the creation of the exciton in pure $ScBO_3$. It agrees well with the results reported by Feofilov.[40] As a rule of thumb, the bottom of the conduction band starts at 1.08 times higher energy, around 7.67 eV. Hence, the situation in $ScBO_3$ is even quantitatively similar to that in $Lu_{0.8}Sc_{0.2}BO_3$. Concerning the $LuBO_3$ calcite phase, the emission spectrum is dominated by the band peaking at 4.13 eV, and the excitation spectrum is clearly high-energy-shifted with respect to that of the 5.17 eV band in $ScBO_3$. Therefore, the excitation band at 7.1 eV in pure $Lu_{0.8}Sc_{0.2}BO_3$ (see Figure 1) is related to the exciton creation near a Sc site, and the mobility edge is related to the charge transfer transition from oxygen ligands to 5d states of Lu^{3+} at about 7.6 eV.

3.2. Energy Transfer from Host to Activator in $Lu_{0.8}Sc_{0.2}BO_3$:Ln^{3+} (Ln = Ce, Pr, Nd, Yb). The X-ray excited emission spectrum of Ce-doped $Lu_{0.8}Sc_{0.2}BO_3$ at room temperature is shown in Figure 3a. The weak band at 4.77 eV, also observed in the pure $Lu_{0.8}Sc_{0.2}BO_3$ (see Figure 3e), is attributed to the STE emission. The typical 5d−4f transition of Ce^{3+} peaking at 3.35 and 3.10 eV could also be clearly observed. The VUV excitation and emission spectra of Ce^{3+} ions are shown in Figure 4. In Figure 4, spectrum a, the weak STE excitation peak at 6.89 eV indicates that the transfer efficiency of excitation energy to Ce^{3+} is rather low, and above 7.75 eV, it starts to increase. Apparently, the unbound electrons and holes in the conduction band and valence band, respectively, transfer the excitation energy more efficiently to Ce than STE does.

In Figure 4, spectra b and c, the emission spectra under the 8.55 eV excitation (a typical band-to-band transition) and 6.89 eV (STE excitation) are shown. The $I(Ce^{3+})$, I(TE and defect),

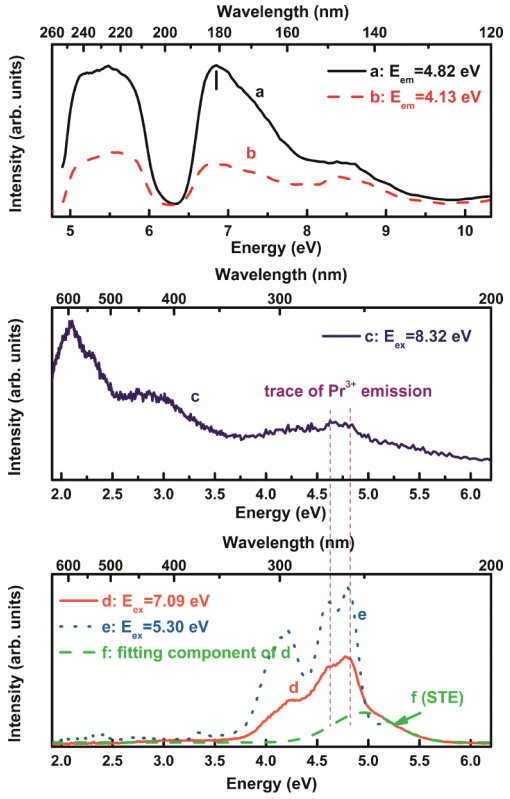

Figure 5. The VUV excitation spectrum (under emission at 4.82 (a) and 4.13 eV (b)) and VUV excited emission spectrum (excitation under 8.32 (c), 7.09 (d), and 5.30 eV (e)) of $Lu_{0.8}Sc_{0.2}BO_3$:0.5 atom % Pr.

and I(STE) are defined as the emission spectrum integral related to the Ce^{3+}, TE, and defect and STE emissions, respectively. Evaluating spectra b and c, we found that the value of $I(Ce^{3+})/I$(TE and defect) is relatively larger than $I(Ce^{3+})/I$(STE). It confirms the above hypothesis that unbound electrons and holes in the conduction band and valence bands, respectively, transfer the excitation energy more efficiently to Ce than STE does.

The excitation spectrum of Ce^{3+} could assign excitation bands to five electronic transitions to the 5d level of Ce^{3+} fundamentally split by an octahedral field, namely, lower-lying triplet T_{2g} and upper-lying doublet E_g, further split by an additional field of lower symmetry. The five excitation bands corresponding to electronic transitions to 5d excited energy levels of Ce^{3+} ion are labeled as $5d_1$, $5d_2$, $5d_3$, $5d_4$, $5d_5$ in Figure 4 spectrum a. Although the locations of $5d_4$ and $5d_5$ excited levels could not be well resolved, the location of $5d_1$, $5d_2$, and $5d_3$ excited levels can be clearly identified at 3.65, 4.07, and 5.15 eV, respectively. In Figure 4, spectrum f, the characteristic Ce doublet peaking at 3.35 and 3.14 nm is similar to that observed in the XEL spectrum. The separation of 1680 cm^{-1} between the subbands is relatively smaller than the expected spin and orbit splitting between the $^2F_{5/2}$ and $^2F_{7/2}$ states (2000 cm^{-1}). The Stokes shift of the emission to the ground state is 2000 cm^{-1}, which is also somewhat smaller in comparison with typical values for Ce^{3+} in other oxide compounds.

In our previous work,[41] we depicted the first tentative scheme with the energy levels of Ce^{3+} placed with respect to the top of the valence and the bottom of the conduction band in the $Lu_{0.8}Sc_{0.2}BO_3$ host. From an Arrhenius plot of the 5d−4f decay

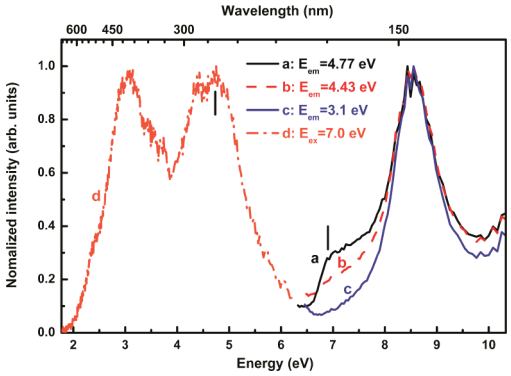

Figure 6. The VUV excitation spectrum (under emission at 4.77 (a), 4.43 (b), and 3.1 eV (c)) and VUV excited emission spectrum (excitation under 7.0 eV (d)) of $Lu_{0.8}Sc_{0.2}BO_3$:1 atom % Yb.

time as a function of the temperature, we estimated that the lowest 5d state is located 0.35 eV below the conduction band edge. This implies that the 4f ground state is ∼3.6 eV above the top of the valence band.

The X-ray excited luminescence spectrum of Pr^{3+}-doped $Lu_{0.8}Sc_{0.2}BO_3$ at room temperature in Figure 3b consists of 5d−4f emission bands between 3.8 and 5.0 eV and weak 4f−4f emission lines between 2.25 and 2.48 eV. The VUV excitation and emission spectra of Pr^{3+}-doped $Lu_{0.8}Sc_{0.2}BO_3$ are shown in Figure 5. In Figure 5, spectrum a, a strong STE excitation peak at 6.89 eV indicates that the transfer efficiency of excitation energy to Pr^{3+} is quite high, and above 7.75 eV, it shows a relative decrease. Apparently, STE transfers excitation energy more efficiently to Pr compared with the unbound electrons and holes in the conduction band and valence bands, respectively. In Figure 5, spectrum c, although the strongest two 5d−4f emissions of Pr^{3+} could be identified, they are hardly distinguishable in the TE and defect emission bands. To some extent, it reveals that the energy transfer efficiency from the host to Pr^{3+} is poor. On the other hand, both the 5d−4f transition of Pr^{3+} and the STE emission can be clearly identified under the excitation at 7.09 eV, which further corroborates the energy transfer from STE to Pr^{3+} ions is more efficient.

In Figure 5, spectrum a, we find that the lowest 5d state of Pr^{3+} is at ∼5.3 eV (234 nm). In Figure 5, spectrum e, the emission bands at 4.84, 4.64, 4.28, and 4.01 eV are identified as emissions from the lowest 4f−5d state to the $^3H_4$, $^3H_5$, [$^3H_6$ and $^3F_2$], and [$^3F_3$ and $^3F_4$] states of Pr^{3+}, respectively.[20] The Stokes shift is calculated to be 0.32 eV.

The excitation of the $4f^2(^1S_0)$ state of Pr^{3+} is at ∼5.79 eV (214 nm). Hence, the relaxed lowest-energy 4f−5d state is located well below this $4f^2(^1S_0)$ state. Photon cascade emission[42] from that state is not possible for Pr^{3+}-doped $Lu_{0.8}Sc_{0.2}BO_3$, and fast emission from the $5d_1$ state is enabled. Moreover, together with the results of our previous work,[41] we can establish the scheme of the Pr^{3+} energy levels within the forbidden gap of $Lu_{0.8}Sc_{0.2}BO_3$. From an Arrhenius plot of the 5d−4f decay time as a function of the temperature,[41] we estimate that the lowest 5d state is located 0.25 eV below the conduction band edge, which implies that the 4f ($^3H_4$) ground state is 2.05 eV above the top of the valence band. This value is 1.55 eV higher energy shift than that of Ce^{3+}, which agrees well with the theoretical value 1.51 ± 0.09 eV.[43]

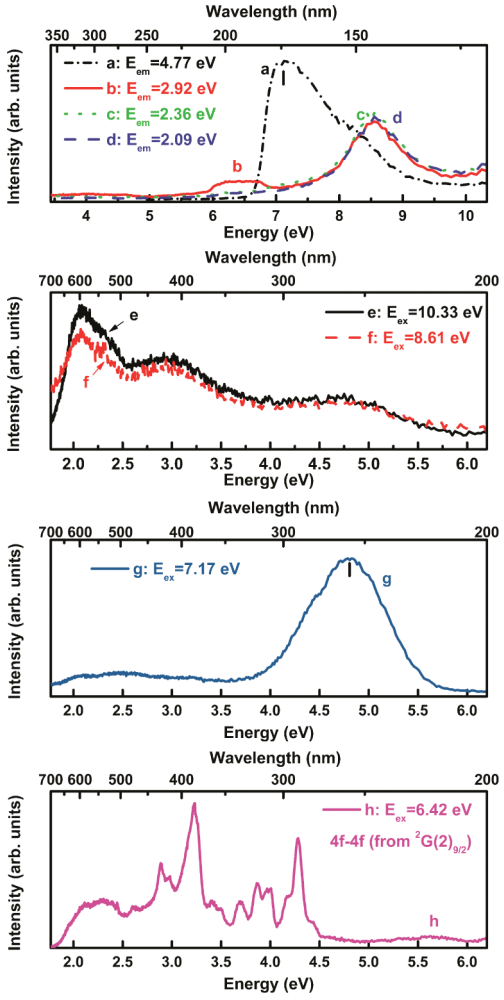

Figure 7. The VUV excitation spectrum (under emission at 4.77 (a), 2.92 (b), 2.36 (c), and 2.09 eV (d)) and VUV excited emission spectrum (excitation under 10.33 (e), 8.61 (f), 7.17 (g), and 6.42 eV (h)) of $Lu_{0.8}Sc_{0.2}BO_3$:1 atom % Nd.

The X-ray excited luminescence spectrum in Figure 3c for Yb^{3+}-doped $Lu_{0.8}Sc_{0.2}BO_3$ at room temperature presents only the STE and TE/defect emission bands, identical to the spectrum of pure $Lu_{0.8}Sc_{0.2}BO_3$. The charge transfer (CT) luminescence of Yb^{3+} is not observed at all at room temperature. In ref 44, it is reported that $LnBO_3$ (Ln=Sc, Y, La) the Yb^{3+} CT luminescence is not observed for any of the orthoborates, even at 10 K. Therefore, it is reasonable to believe that the Yb^{3+} CT luminescence in the $Lu_{0.8}Sc_{0.2}BO_3$ host has also been completely quenched at room temperature. The VUV excitation and emission spectra shown in Figure 6 are similar to the spectra of pure $Lu_{0.8}Sc_{0.2}BO_3$ without any sign of the Yb^{3+} CT luminescence. qIt is also worth mentioning that another obstacle to Yb^{3+} CT luminescence appearance might be the competition between the electron capture around Yb^{3+} and Sc^{3+} ions under X-ray excitation.

The X-ray excited luminescence spectrum in Figure 3d for Nd^{3+}-doped $Lu_{0.8}Sc_{0.2}BO_3$ at room temperature presents only the STE and TE/defect emission bands, identical to the spectrum of pure $Lu_{0.8}Sc_{0.2}BO_3$. However, the $5d^14f^2-4f^3$ emission of Nd^{3+} could not be observed at all; the VUV excitation and emission spectra of Nd^{3+} in $Lu_{0.8}Sc_{0.2}BO_3$ are shown in Figure 7.

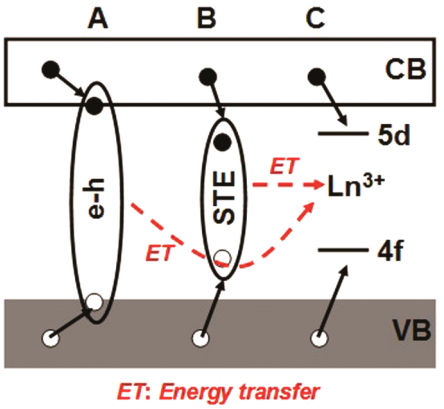

Figure 8. Scheme of the various characteristic emissions and energy transfer processes occurring in $Lu_{0.8}Sc_{0.2}BO_3$:Ln^{3+}, Ln = Ce, Pr. In the absence of Ln, free charge carriers trap around defects (A) or form a STE localized around the Sc site (B). When the Ln^{3+} ion is introduced, recombination of free carriers takes place, mostly through the dopant (c), which quenches the other emissions mentioned. The e−h pathway must be changed to a TE/defect center and show an even deeper level of relaxation with respect to STE.

Therefore, we conclude that, in contrast to the case of Ce^{3+} and Pr^{3+}, the energy transfer pathways from both the host and STE toward Nd^{3+} are inefficient.

The Nd^{3+} excitation spectrum (E_{em} = 2.92 eV) (Figure 7 spectrum b) shows a band around 6.42 eV (193 nm) that can be ascribed to the transition from the lowest energy 5d state of Nd^{3+}. Usually the lowest 5d state of Nd^{3+} is ∼ 2.80 eV higher energy than that for Ce^{3+}.[45] In our case, the energy shift is 2.82 eV, which matches well the theoretical value. Moreover, Figure 7, spectrum g, shows that excitation at 6.42 eV leads to f−f emission lines and additional broad bands. The latter ones, already observed under 10.33 and 8.86 eV excitations (Figure 7 spectrum d and e) can be attributed to TE/defect emissions. For Nd^{3+}-doped $Lu_{0.8}Sc_{0.2}BO_3$, no d−f emission is observed due to an efficient nonradiative relaxation from the lowest $4f^25d$ to a $4f^3$ ($^2G_{7/2}$) level, leading to f−f emission.[46]

In Figure 8, we summarize our findings in the form of a simple sketch with the following comments:

(i) Excitation of electrons up to the conduction band leads to the/defect-based luminescence (A).

(ii) When the Ce^{3+} (Pr^{3+}) ion is introduced to the $Lu_{0.8}Sc_{0.2}BO_3$ host, the free electron and holes partly recombine around the doped ions (C), whose emission appears at the expense of process A.

(iii) The STE localized at the Sc site (B) is preferably created under excitation in the exciton absorption band around 180 nm and emits its characteristic luminescence. This process is also partially diminished by introducing Ce^{3+} (Pr^{3+}) ions.

(iv) For Nd^{3+}- and Yb^{3+}-doped ions, the energy transfer mechanism from the host is quite different, which may be due to the possible/preferred electron capture at these ions and their specific de-excitation pathways.:

The energy transfer from STE to Ce^{3+} (Pr^{3+}) ions exists for both the VUV and X-ray excitation. In contrast, the energy transfer from STE to Nd^{3+} ions is utterly inefficient. The efficiency of this process is defined by the overlap of the STE emission band with the 4f−5d absorption band of these dopants,

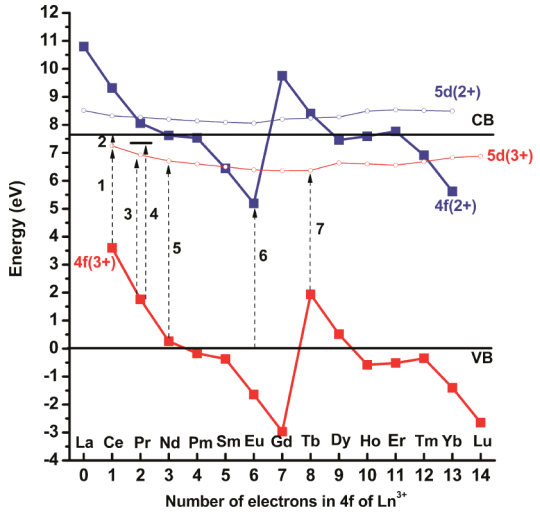

Figure 9. Energy level schemes of divalent and trivalent lanthanides in $Lu_{0.8}Sc_{0.2}BO_3$. The dashed arrows indicate experimental f−d transitions (nos. 1, 3, 4, 5, 7), charge transfer transitions (no. 6), and thermal activation energy (no. 2) discussed in the text. Positions of the experimental and predicted energy levels of the 5d state of Pr^{3+} are indicated by arrows nos. 4 and 3, respectively.

which is described by the Forster−Dexter energy transfer model. The efficient energy transfer via STE to Eu^{3+} and Tb^{3+}[22] further corroborate the above analysis. The energy transfer by direct electron−hole capture at Ce^{3+} or Pr^{3+} ions is efficient under X-ray excitation. It means that, compared with the excitation in the exciton absorption band, the Ce^{3+} and Pr^{3+} ions compete more efficiently for the energy of migrating charge carriers. The recombination of e−h pairs through Nd^{3+} ions is inefficient, possibly as a result of the reversed order of charge carrier capture (see below).

3.3. Energy Level Diagrams of Divalent and Trivalent Lanthanides in $Lu_{0.8}Sc_{0.2}BO_3$ Host. Figure 9 shows a predictive energy level diagram of divalent and trivalent lanthanides in $Lu_{0.8}Sc_{0.2}BO_3$, which is constructed by using a three-parameter model[24] and the latest parameters[45] developed by Dorenbos. The top of the valence band is defined as the zero of energy. The detailed entry information for the three-parameter model is listed as follows:

(i) The band gap energy between the top of the valence band and the bottom of the conduction band has been evaluated to ∼7.6 eV. The band gap energy corresponds to the creation of a free electron in the conduction band and a free hole in the valence band. Let us consider the spectroscopic redshift of the f−d transition. Because of a strong interaction between the 5d electron and host lattice, the spectroscopic red shift is defined as the energy shift of the lowest 5d state of a lanthanide in a compound in comparison with the energy of the free lanthanide ion. A good estimation could be made from the red shift value for trivalent lanthanides. One obtains a red shift value of 2.47 eV for $Lu_{0.8}Sc_{0.2}BO_3$:Ce^{3+} from the energy value of 3.65 eV for the first $4f^1 \rightarrow 5d^1$ transition labeled by arrow 1 in Figure 9 because the same transition of free Ce^{3+} is 6.12 eV.[24] However, the red shift is usually not available for divalent lanthanides at trivalent lattice sites,[47] but a good estimate can be made from the equation $D(2+, A) = 0.64D(3+, A) - 0.233$ eV, where $D(2+, A)$ and $D(3+, A)$ are the red shift in divalent and trivalent lanthanides, respectively. Therefore, the red shift of the f−d transition of the divalent ion is estimated at 1.35 eV.

(ii) The energy of charge transfer from the valence band of $Lu_{0.8}Sc_{0.2}BO_3$ to Eu^{3+}, which is close to the energy gap between the top of the valence band and the ground state $4f^7$ of Eu^{2+}. The data presented in the literature[22] leads to a value of 5.19 eV (239 nm). Although it is a speculative assignment, it is in good agreement with the results reported by Koike[48] for the Eu^{3+} CT band in $LuBO_3$ and $ScBO_3$ host, about 220−230 nm. Arrow 6 in Figure 9 represents this charge transfer. The energy difference between the charge transfer to Eu^{3+} and to other trivalent lanthanides is independent of the host lattice, such as oxide and fluoride compounds.[24] Because of the quenching of charge transfer emission of Yb^{3+} at room temperature, we could not obtain the Yb^{2+} 4f level position. Nevertheless, thanks to the charge transfer energy of Eu^{3+} in the $Lu_{0.8}Sc_{0.2}BO_3$ host, one may calculate the curve labeled Ln^{2+} 4f in Figure 9, which represents the $4f^{n+1}$ ground states of all divalent lanthanides in the $Lu_{0.8}Sc_{0.2}BO_3$ host. Then, the red shift for divalent lanthanides (1.35 eV) allows us to determine the energy of the lowest 5d level in divalent lanthanides relative to the $4f^{n+1}$ ground state. Combined with the energy of the lowest 5d level for each divalent free lanthanide, the lowest 5d level for each divalent lanthanide in $Lu_{0.8}Sc_{0.2}BO_3$ host is built in Figure 9. Due to the 5d levels located in the conduction band, no d−f emissions are expected for Ln^{2+} ions in $Lu_{0.8}Sc_{0.2}BO_3$ host.

The energy levels of trivalent lanthanides can be built in the identical way.[24] So far, the band gap energy between the top of the valence band and the bottom of the conduction band and the red shift of the f−d transition for trivalent lanthanides in the $Lu_{0.8}Sc_{0.2}BO_3$ host have been discussed and obtained. In addition, another parameter is also needed for the purpose of locating the $4f^n$ ground state or a $4f^{n-1}5d^1$ excited level of one of the Ln^{3+} ions with respect to the valence band or the conduction band.

For example, the energy gap between the lanthanide ion ground state and the host conduction band can be deduced by photoluminescence and decay time measurements as a function of temperature.[30−32] Specifically, the energy difference between the lowest $5d_1$ excited level of Ce^{3+} and the conduction band can be deduced from the temperature dependence of Ce^{3+} nanosecond decay times,[49] which become shorter due to an autoionization process. For Ce^{3+} in the $Lu_{0.8}Sc_{0.2}BO_3$ host, we have located the lowest 5d excited level at an energy of 0.35 eV below the conduction band, as sketched in Figure 9 with arrow 2. On the basis of the location of the lowest 5d level of Ce^{3+}, the location of the lowest 5d level of the other trivalent lanthanide ions can be estimated, and then the curve labeled Ln^{3+} 5d can be constructed.

Finally from red shift values, the energy differences between the lowest 5d state and the 4f ground state for each trivalent lanthanide could be derived, and then this leads to the curve labeled Ln^{3+} 4f in Figure 9. On the basis of the VUV data, we have obtained the 5d−4f transition of Nd^{3+} and Tb^{3+}: 6.5 and 4.5 eV, respectively. These values are in excellent agreement with the predictive data derived from the energy diagram (see arrow 5 for Nd^{3+} and arrow 7 for Tb^{3+}).

By using the three-parameter model, a complete energy level diagram is established for all divalent and trivalent lanthanides in

the $Lu_{0.8}Sc_{0.2}BO_3$ host. Although the effectiveness of the diagram constructed by the three-parameter model to predict the optical properties and interpret spectroscopic results has been corroborated by our work and other scientists,[50−53] this model indeed has some uncertainties. For example, with an increase in the temperature, the band gap value could be modified, and consequently, it may induce some error. Interestingly, the position of the Pr^{3+} $5d_1$ lowest state determined experimentally in the same way as for Ce^{3+} above is ∼0.4 eV high energy-shifted compared with the predicted position, which is considered equal to or lower than that of Ce^{3+}. However, for several other oxide hosts, such as Lu_2SiO_5,[31] Y_2SiO_5,[54] and $Lu_2Si_2O_7$,[55,56] it is also not the case. Nevertheless, van der Kolk[57] convincingly concluded that a $4f5d \rightarrow 4f^2$ intersystem crossing lowers the effective ionization barrier so that the lowest-energy 5d state of Pr^{3+} can still be positioned at the same energy below the CB as Ce^{3+} in the LSO and YSO host. However, Nikl discovered that there is a delayed radiative recombination process in Pr^{3+}-doped scintillators, such as LSO:Pr^{3+},[31] YSO:Pr^{3+},[54] and LPS:Pr^{3+},[55] which meant the $4f5d \rightarrow 4f^2$ intersystem crossing should be negligible. Since their standpoints were both strongly supported by their respective experiments, one may wonder whether both the intersystem crossing and the delay radiative recombination process exert effects on the Pr^{3+}-doped scintillators. Thus, the related study deserves to be further investigated.

4. CONCLUSIONS

The undoped $Lu_{0.8}Sc_{0.2}BO_3$ presents two different emissions upon excitation at energies in the vicinity of the band gap or under X-ray. The emission at the high energy side, located at 4.77 eV, is ascribed to self-trapped exciton, which is anchored by electron capture around the Sc site. We also observe three broad band emissions at 4.43, 3.02, 2.10 eV, which are attributed to the trapped exciton or at-the-defect recombination emission. Two energy transfer pathways in Ln^{3+}-doped $Lu_{0.8}Sc_{0.2}BO_3$ are found: namely, the energy transfer from STE to Ln^{3+} ions and the energy transfer by direct electron−hole capture on Ln^{3+} ions. The energy transfer from STE to Ln^{3+} ions is conditioned by the overlap of the self-trapped exciton emission and Ln^{3+} absorption bands. For the Ce^{3+}- and Pr^{3+}-doped samples, the host-to-activator energy transfer is dominated by charge carrier capture upon excitation by X-ray. The Yb^{3+} CT luminescence was not observed at room temperature. Finally, the predictive energy level diagrams for divalent and trivalent lanthanides in $Lu_{0.8}Sc_{0.2}BO_3$ were successfully constructed by using the three parameter method.

AUTHOR INFORMATION

Corresponding Author

*Phone: +86 021 69987740. Fax: +86 021 59927184. E-mails: rgh@mail.sic.ac.cn (G.H.R.); caswyt@hotmail.com (Y.T.W.).

ACKNOWLEDGMENT

The authors thank beamline BS-U10B of the National Synchrotron Radiation Laboratory of China for providing the beam time. This work is supported by the National Natural Science Foundation of China (Grant No. 50902145), and support in part of the Sino−Czech Scientific & Technological Cooperation Committee project (Czech MSMT KONTAKT Grant ME10084) is also gratefully acknowledged.

REFERENCES

(1) Weber, M.J.; Derenzo, S.E.; Dujardin, C.; Moses, W.W. In *Proceedings of the International Conference on Inorganic Scintillators and Their Applications*, September 1995, p 325.

(2) Moses, W.W.; Weber, M.J.; Derenzo, S.E.; Perry, D.; Berdahl, P. In *Proceedings of the International Conference on Inorganic Scintillators and Their Applications*, September 1997, p 22.

(3) Zhang, L.; Pedrini, C.; Madej, C.; Dujardin, C.; Gâcon, J. C.; Moine, B.; Kamenskikh, I.; Belsky, A.; Shaw, D. A.; MacDonald, M. A.; Mesnard, P.; Fouassier, C.; Van't Spijker, J. C.; Van Eijk, C. E. W. *Radiat. Eff. Defects Solids* **1999**, *150*, 47.

(4) Boyer, D.; Leroux, F.; Bertrand, G.; Mahiou, R. *J. Non-Cryst. Solids* **2002**, *306*, 110.

(5) Chadeyron-Bertrand, G.; Boyer, D.; Dujardin, C.; Mansuy, C.; Mahiou, R. *Nucl. Instrum. Methods Phys. Res. B.* **2005**, *229*, 232.

(6) Mansuy, C.; Tomasell, E.; Mahiou, R.; Gengembre, L.; Grimblot, J.; Nedelec, J. M. *Thin Solid Films* **2006**, *515*, 666.

(7) Mansuy, C.; Nedelec, J. M.; Mahiou, R. *J. Mater. Chem.* **2004**, *14*, 3274.

(8) Yang, J.; Li, C. X.; Zhang, X. M.; Quan, Z. W.; Zhang, C. M.; Li, H. Y.; Lin, J. *Chem.—Eur. J.* **2008**, *14*, 4336.

(9) Levin, E.; Roth, R. S.; Martin, J. B. *Am. Mineral.* **1961**, *46*, 1030.

(10) Wu, Y. T.; Ding, D. Z.; Pan, S. K.; Yang, F.; Ren, G. H. *Phase Transitions* **2011**, *84*, 315.

(11) Wu, Y.T.; Ding, D.Z.; Yang, F.; Pan, S.K.; Ren, G.H.; , *Mater. Res. Bull.* **2011**, doi:10.1016/j.materresbull.2011.09.023.

(12) Hatamoto, S.; Yamazaki, T.; Hasegawa, J.; Katsurayam, M.; Oshika, M.; Anzai, Y. *J. Cryst. Growth* **2009**, *311*, 530.

(13) Yanagida, T.; Fujimoto, Y.; Kawaguchi, N.; Yokota, Y.; Kamada, K.; Totsuka, D.; Hatamoto, S.; Yoshikawa, A.; Chani, V. *Nucl. Instrum. Methods. Phys. Res. A* **2010**, doi:10.1016/j.nima.2010.08.115.

(14) Wu, Y. T.; Ding, D. Z.; Pan, S. K.; Yang, F.; Ren, G. H. *J. Alloys Compd.* **2011**, *509*, 366.

(15) Wu, Y. T.; Ding, D. Z.; Pan, S. K.; Yang, F.; Ren, G. H. *Cryst. Res. Technol.* **2011**, *46*, 48.

(16) Wu, Y. T.; Ding, D. Z.; Pan, S. K.; Yang, F.; Ren, G. H. *Opt. Mater.* **2011**, *33*, 655.

(17) Wu, Y. T.; Ding, D. Z.; Pan, S. K.; Yang, F.; Ren, G. H. *Mater. Sci. Eng., B* **2011**, *176*, 889.

(18) Lempicki, A.; Wojtowicz, A.; Berman, E. *Nucl. Instrum. Methods Phys. Res. A* **1993**, *333*, 304.

(19) Robbins, D. *J. Electrochem. Soc.* **1980**, *127*, 2694.

(20) Drozdowski, W.; Wisniewski, D.; Wojtowicz, A.; Lempicki, A.; Dorenbos, P.; de Haas, J.; van Eijk, C.; Bos, A. *J. Lumin.* **1997**, *72−74*, 756.

(21) Wu, Y. T.; Ding, D. Z.; Pan, S. K.; Yang, F.; Ren, G. H. *J. Alloys Compd.* **2011**, *509*, 7139.

(22) Wu, Y. T.; Ding, D. Z.; Pan, S. K.; Yang, F.; Ren, G. H. *J. Alloys Compd.* **2011**, *509*, 7186.

(23) Zych, E.; Trojan-Piegza, J. *Chem. Mater.* **2006**, *18*, 2194.

(24) Dorenbos, P. *J. Phys.: Condens. Matter* **2003**, *15*, 8417.

(25) Dorenbos, P.; van der Kolk, E. *Appl. Phys. Lett.* **2006**, *89* (061122), 1–3.

(26) Dorenbos, P.; Shalapska, T.; Stryganyuk, G.; Gektin, A.; Voloshinovskii, A. *J. Lumin.* **2011**, *131*, 633.

(27) Dorenbos, P.; Bos, A. J. J. *Radiat. Meas.* **2008**, *43*, 139.

(28) Dorenbos, P.; Bos, A. J. J.; Poolton, N. R. J. *Phys. Rev. B* **2010**, *82*, 195127.

(29) Pidol, L.; Viana, B.; Galtayries, A.; Dorenbos, P. *Phys. Rev. B* **2005**, *72*, 125110.

(30) Nikl, M.; Begnamini, A. M.; Jary, V.; Niznansky, D.; Mihokova, E. *Phys. Status Solidi RRL* **2009**, *3*, 293.

(31) Nikl, M.; Ogino, H.; Yoshikawa, A.; Mihokova, E.; Pejchal, J.; Beitlerova, A.; Novoselov, A.; Fukuda, T. *Chem. Phys. Lett.* **2005**, *410*, 218.
(32) Nikl, M.; Pazzi, G. P.; Fabeni, P.; Mihokova, E.; Pejchal, J.; Ehrentraut, D.; Yoshikawa, A.; Williams, R. T. *J. Lumin.* **2009**, *129*, 1564.
(33) Wang, Y. H.; Guo, X.; Endo, T.; Murakami, Y.; Ushirozawa, M. *J. Solid State Chem.* **2004**, *177*, 2242.
(34) Wang, Y. H.; Wang, L. L. *Mater. Lett.* **2006**, *60*, 2645.
(35) Zeng, X. Q.; Im, S.; Jang, S.; Kim, Y.; Park, H.; Son, S.; Hatanaka, H.; Kim, G.; Kim, S. *J. Lumin.* **2006**, *121*, 1.
(36) Kucera, M.; Nikl, M.; Prusa, P.; Mares, J. A.; Nitsch, K.; Hanus, M.; Onderisinova, Z.; Kucekova, R. *J. Cryst. Growth* **2011**, *318*, 813.
(37) Ryskn, N. N.; Dorenbos, P.; van Eijk, C. W. E.; Batygov, S. K.H. *J. Phys.: Condens. Matter* **1995**, *6*, 10423.
(38) Zorenko, Y.; Gorbenko, V.; Voznyak, T.; Zorenko, T.; Nikl, M.; Nejezchleb, K. *J. Lumin.* **2008**, *128*, 595.
(39) Nikl, M.; Tous, J.; Mares, J. A.; Prusa, P.; Mihokova, E.; Blazek, K.; Vedda, A.; Zorenko, Yu.; Gorbenko, V.; Babin, V. *Proc. SPIE* **2009**, *7310*, 731008.
(40) Feofilov, S. P.; Zhou, Y.; Jeong, J. Y.; Keszler, D. A.; Meltzer, R. S. *J. Lumin.* **2007**, *125*, 80.
(41) Wu, Y. T.; Nikl, M.; Ding, D. Z.; Yang, F.; Pan, S. K.; Ren, G. H. *Phys. Lett. A*; submitted.
(42) Vink, A. P.; Dorenbos, P.; van Eijk, C. W. E. *J. Solid State Chem.* **2003**, *171*, 308–312.
(43) Dorenbos, P. *J. Phys.: Condens. Matter* **2003**, *15*, 6249.
(44) van Pieterson, L.; Heeroma, M.; de Heer, E.; Meijerink, A. *J. Lumin.* **2000**, *91*, 177.
(45) Dorenbos, P.; Krumpel, A. H.; van der Kolk, E.; Boutinaud, P.; Bettinelli, M.; Cavalli, E. *Opt. Mater.* **2010**, *32*, 1681.
(46) Wegh, R. T.; van Klinken, W.; Meijerink, A. *Phys. Rev. B* **2001**, *64*, 045115.
(47) Dorenbos, P. *J. Phys.: Condens. Matter* **2003**, *15*, 4797.
(48) Koike, J.; Kojima, T.; Toyonaga, R.; Kagami, A.; Hase, T.; Inaho, S. *J. Electrochem. Soc.* **1979**, *126*, 1008.
(49) Lyu, L. J.; Hamilton, D. S. *J. Lumin.* **1991**, *48&49*, 251.
(50) Liu, G. K.; Jensen, M. P.; Almond, P. M. *J. Chem. Phys.* **2006**, *110*, 2081.
(51) Aitasalo, T.; Holsa, J.; Jungner, H.; Lastusaari, M.; Niittykoski, J. *J. Phys. Chem. B* **2006**, *110*, 4589.
(52) Yamaga, M.; Masui, Y.; Sakuta, S. *Phys. Rev. B* **2005**, *71*, 205102.
(53) Yen, W. M. *Phys. Solid State* **2005**, *47*, 1393.
(54) Pejchal, J.; Nikl, M.; Mihokova, E.; Novoselov, A.; Yoshikawa, A.; Williams, R. T. *J. Lumin.* **2009**, *129*, 1857.
(55) Nikl, M.; Ren, G. H.; Ding, D. Z.; Mihokova, E.; Jary, V.; Feng, H. *Chem. Phys. Lett.* **2010**, *493*, 72.
(56) Pidol, L.; Kahn-Harari, A.; Viana, B.; Ferrand, B.; Dorenbos, P.; de Haas, J. T. M.; van Eijk, C. W. E.; Virey, E *J. Phys.: Condens. Matter* **2003**, *15*, 2091.
(57) van der Kolk, E; Dorenbos, P.; van Eijk, C. W. E.; Basun, S. A.; Imbusch, G. F.; Yen, W. M. *Phys. Rev. B* **2005**, *71*, 165120.